

A general model for frictional contacts in colloidal systems

Kay Hofmann,^{1,*} Kay-Robert Dormann,^{2,†} Benno Liebchen,² and Friederike Schmid^{1,‡}

¹*Institute for Physics, Johannes Gutenberg-Universität Mainz, 55099 Mainz, Germany*

²*Institute for Condensed Matter Physics, Department of Physics,
Technische Universität Darmstadt, 64289 Darmstadt, Germany*

(Dated: July 2025)

In simulations of colloidal matter, frictional contacts between particles are often neglected. For spherical colloids, such an approximation can be problematic, since frictional contacts couple translational and rotational degrees of freedom, which may affect the collective behavior of, e.g., colloids under shear and chiral active matter. Deterministic models for frictional contacts have been proposed in the granular matter community. On the colloidal scale, however, thermal fluctuations are important and should be included in a thermodynamically consistent manner. Here, we derive the correct fluctuation-dissipation relation for linear and nonlinear instantaneous frictional contact interactions. Among other, this generates a new generalized class of dissipative particle dynamics (DPD) thermostats with rotation-translation coupling. We demonstrate effects of frictional contact interactions using the examples of Poiseuille flow and motility induced phase separation in active Langevin particles.

I. INTRODUCTION

Friction has been studied for centuries. Early important observations of frictional forces acting on macroscopic bodies on surfaces have been made by da Vinci and Amontons¹. In the 18th century, Coulomb discovered his famous friction law². Later, the role of frictional contacts between particles in many particle systems has also been intensively explored in granular matter. Here, friction induces a significant coupling between translational and rotational degrees of freedom of the particles. Commonly employed standard models describing frictional contacts in granular matter have been discussed in Refs. ³⁻⁶. Characteristically, these models do not account for thermal fluctuations, which are negligibly weak for granular particles. A first model to describe dry friction in Brownian particles has been developed by de Gennes in 2005⁷. This paper also proposes an experimental realization based on granular particles in randomly vibrating plates. Such situations, which involve both frictional contacts and imposed Brownian motion, have subsequently been studied both theoretically and experimentally⁸⁻¹¹ and very recently also in (granular) active particles¹².

At the colloidal scale, frictional contacts have long been neglected. However, within the past decade, there has been increasing evidence that frictional contacts can play an important role in colloidal systems, in particular when they are sheared, leading to large relative velocities of adjacent colloids. In particular, the role of frictional contacts for discontinuous shear thickening in colloidal (and larger) particles has been prominently discussed. While discontinuous shear-thickening has originally been attributed to lubrication flows¹³, later

theoretical¹⁴⁻¹⁶ and experimental¹⁷⁻²¹ works provide evidence, that (nanoscale) repulsive and frictional forces play a key role for discontinuous shear-thickening. A popular idea is that at low pressure, the solvent in the gaps between adjacent particles keeps them apart, whereas at higher pressure, the particles overcome repulsive forces and frictional contacts become important, ultimately resulting in shear thickening. While the overall mechanism for the emergence of discontinuous shear thickening is probably comparatively involved²², there is now strong evidence that frictional contacts play a central role for sheared colloids undergoing discontinuous shear-thickening.

Recently, frictional contacts have also been intensively studied in (colloidal) active matter systems. Similarly as in sheared systems, also in active systems the relative velocity between adjacent particles can be rather high, suggesting that frictional contacts could play an important role in these systems²³. To describe frictional contacts, Nie et al²³ have employed a model from the granular community, whereas Abaurrea-Velasco et al^{24,25} have developed a new model describing overdamped active particles with frictional contacts. Besides self-propelled active particles, also active spinners with frictional contacts have been studied²⁶.

Importantly, unlike for granular matter, for colloidal matter thermal fluctuations are important. Despite this, most models that have been used to describe frictional contacts in colloidal matter have borrowed models to describe friction from the granular community^{3,6}, or have developed new ones^{24,25} which have been combined with standard translational and rotational additive white noise terms, similarly as for particles without frictional contacts. This may be sufficient to describe common experiments, but from a fundamental perspective, this approach leads to thermodynamically inconsistent models that may violate Onsager relations and do not obey the fluctuation dissipation theorem in the equilibrium limit. This happens for models that account only for fluctua-

* khofmann@uni-mainz.de

† kay-robert.dormann@pkm.tu-darmstadt.de

‡ friederike.schmid@uni-mainz.de

tions that appear as a counterpart to Stokes drag, but not for the additional fluctuations that necessarily arise as a counterpart to tangential friction (frictional contacts) in colloids that are subject to a thermal bath. As we show in the present work, thermodynamic inconsistencies due to the consideration of incomplete thermal fluctuations can (wrongly) lead to the prediction of different equilibrium temperature values for the rotational and translational degrees of freedom, which both differ from the bath temperature. In nonequilibrium, for active systems, thermodynamically inconsistent treatments of frictional contacts can even lead to non-Maxwell-Boltzmann velocity distributions and can have severe consequences for the predicted collective behaviour.

The central aim of the present work is therefore to develop a thermodynamically consistent model to describe colloidal matter with frictional contacts (active and passive). To achieve this, we develop a model that is closely related to a popular model from the granular community⁵ and systematically calculate the required *multiplicative* noise term. Using particle based simulations, we confirm that the resulting translational and angular velocity distributions are fully consistent with the predictions from statistical mechanics and both lead to temperatures that coincide with the bath temperature. To exemplarily study the role of thermodynamic (in)consistencies, we explore two examples for sheared colloids and for active colloids undergoing motility-induced phase separation.

Our results could serve as a useful ingredient to model sheared colloidal suspensions, to help understand discontinuous shear thickening and to model systems of self-propelled particle as well as active spinners with frictional contacts. The latter should be of particular interest in the context of the enormous present interest in odd hydrodynamics²⁷.

II. RESULTS

A. Theory: Modeling tangential friction interactions

1. Statement of the problem

We consider systems of spherical colloidal particles that interact with each other via conservative forces and surface friction forces. In addition, the particles may interact with a background medium and/or experience further driving or active forces. Specific examples will be discussed in Section II B. Here, we focus on the modeling of the surface friction forces.

The friction forces depend on the relative tangential velocities of the particles at the point of contact, but not necessarily in a linear manner. If two particles collide, this induces changes of both their momenta and angular momenta. As mentioned in the introduction, deterministic models for such contact forces have been discussed for centuries. On colloidal scales, however, an additional

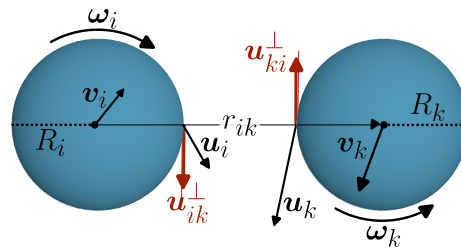


FIG. 1. Sketch of two-particle configuration subject to tangential friction

aspect comes in: Thermal fluctuations become important. Friction forces are invariably associated with random, stochastic forces, which can not be ignored on small scales, but must be included in a thermodynamically consistent manner. To ensure that passive systems without nonequilibrium driving forces reach thermal equilibrium, the frictional and the corresponding stochastic forces must satisfy a fluctuation-dissipation relation. In other words: the frictional and stochastic forces must be coupled such that, together, they act as a thermostat for the system, independent of other thermostats that may describe, e.g., the coupling to a background medium.

Our aim is to derive a general structure of thermostats that arise from tangential friction forces between particles. We will focus on Markovian forces without memory. In the granular matter literature, non-Markovian friction models have also been proposed to mimic transitions between static and dynamic friction^{4,5}. Such models will not be considered here.

2. Structure of deterministic friction force

The general form of deterministic Markovian tangential friction forces between two spherical particles i and k with radii $R_{i,k}$, center positions $\mathbf{r}_{i,k}$, angular velocities $\boldsymbol{\omega}_{i,k}$, and total velocities $\mathbf{v}_{i,k}$, can be constructed as follows.⁴ If the particles are in contact, their surface velocities at the contact point are given by

$$\mathbf{u}_i = \mathbf{v}_i + \boldsymbol{\omega}_i \times \hat{\mathbf{r}}_{ik} R_i \quad (1)$$

$$\mathbf{u}_k = \mathbf{v}_k - \boldsymbol{\omega}_k \times \hat{\mathbf{r}}_{ik} R_k, \quad (2)$$

where we have defined $\hat{\mathbf{r}}_{ik} = \mathbf{r}_{ik}/r_{ik}$ with $\mathbf{r}_{ik} = \mathbf{r}_k - \mathbf{r}_i$ and $r_{ik} = |\mathbf{r}_{ik}|$. From these expressions, we can calculate the relative tangential velocity \mathbf{u}_{ik}^\perp at the contact point as the projection of the surface velocity difference, $\mathbf{u}_k - \mathbf{u}_i$, onto the tangent plane at contact (see Fig. 1), i.e., $\mathbf{u}_{ik}^\perp = \mathbf{P}(\hat{\mathbf{r}}_{ik})(\mathbf{u}_k - \mathbf{u}_i)$ with the projection operator

$$\mathbf{P}(\hat{\mathbf{r}}_{ik}) = \mathbf{1} - \hat{\mathbf{r}}_{ik} \hat{\mathbf{r}}_{ik}, \quad (3)$$

giving

$$\mathbf{u}_{ik}^\perp = \mathbf{P}(\hat{\mathbf{r}}_{ik})(\mathbf{v}_k - \mathbf{v}_i) - (\boldsymbol{\omega}_i R_i + \boldsymbol{\omega}_k R_k) \times \hat{\mathbf{r}}_{ik}. \quad (4)$$

Assuming that the tangential friction force at the contact point points in the direction of \mathbf{u}_{ik}^\perp , we model it very generally as

$$\mathbf{F}_i^{\text{f,contact}} = -\mathbf{F}_k^{\text{f,contact}} = f(u_{ik}^\perp, r_{ik}) \hat{\mathbf{u}}_{ik}^\perp \quad (5)$$

with $\hat{\mathbf{u}}_{ik}^\perp := \mathbf{u}_{ik}^\perp / u_{ik}^\perp$, where $f(u_{ik}^\perp, r_{ik})$ is an arbitrary function of the relative tangential velocity and the distance between the particles. The surface force $\mathbf{F}_i^{\text{f,contact}}$ generates a center-of-mass force and torque acting on particle i ,

$$\mathbf{F}_{ik}^{\text{f}} = \mathbf{F}_i^{\text{f,contact}}, \quad \boldsymbol{\tau}_{ik}^{\text{f}} = R_i \hat{\mathbf{r}}_{ik} \times \mathbf{F}_i^{\text{f,contact}}, \quad (6)$$

which is a pair friction force and torque resulting from the friction with the particle k and can be rewritten as

$$\mathbf{F}_{ik}^{\text{f}} = \frac{f(u_{ik}^\perp, r_{ik})}{u_{ik}^\perp} [\mathbf{P}(\hat{\mathbf{r}}_{ik})(\mathbf{v}_k - \mathbf{v}_i) + \hat{\mathbf{r}}_{ik} \times (\boldsymbol{\omega}_i R_i + \boldsymbol{\omega}_k R_k)], \quad (7)$$

$$\frac{\boldsymbol{\tau}_{ik}^{\text{f}}}{R_i} = \frac{f(u_{ik}^\perp, r_{ik})}{u_{ik}^\perp} [\hat{\mathbf{r}}_{ik} \times (\mathbf{v}_k - \mathbf{v}_i) - \mathbf{P}(\hat{\mathbf{r}}_{ik})(\boldsymbol{\omega}_i R_i + \boldsymbol{\omega}_k R_k)]. \quad (8)$$

We note that the torques transmitted to the two particles i and k point in the same direction (and are in fact identical for $R_i = R_k$), whereas the forces are opposed to each other. One can easily see that the deterministic friction force always reduces the kinetic energy of the two particles during a collision, since

$$\begin{aligned} \left. \frac{d}{dt} E_{\text{kin}} \right|_{\text{f}} &= \left. \frac{d}{dt} \frac{1}{2} (m_i \mathbf{v}_i^2 + m_k \mathbf{v}_k^2 + \boldsymbol{\omega}_i \mathbf{I}_i \boldsymbol{\omega}_i + \boldsymbol{\omega}_k \mathbf{I}_k \boldsymbol{\omega}_k) \right|_{\text{f}} \\ &= \mathbf{F}_{ik}^{\text{f}} \cdot (\mathbf{v}_i - \mathbf{v}_k) + \boldsymbol{\tau}_{ik}^{\text{f}} \cdot \boldsymbol{\omega}_i + \boldsymbol{\tau}_{ki}^{\text{f}} \cdot \boldsymbol{\omega}_k \\ &= -f(u_{ik}^\perp, r_{ik}) u_{ik}^\perp \leq 0, \end{aligned} \quad (9)$$

where $m_{i,k}$ are the masses, $\mathbf{I}_{i,k}$ the moments of inertia of the two particles, and the subscript f refers to the fact that only the effect of friction forces is considered. No energy is dissipated in this model if $\mathbf{u}_{ik}^\perp = 0$, which corresponds to a rolling contact. Furthermore, the possibility of spinning friction is also neglected.

In addition to our analytical derivation, we have numerically verified that energy is dissipated during particle collisions (Supplementary Fig. S1).

3. Structure of corresponding stochastic force

Our goal is to construct stochastic forces such that, together with the deterministic friction forces, the configurations are Boltzmann distributed at equilibrium. To this end, we examine the corresponding Fokker-Planck equation.²⁸

The system of interest consists of N particles with positions \mathbf{r}_i , orientations characterized by two orthogonal unit vectors ($\mathbf{e}_i^{(1)}, \mathbf{e}_i^{(2)}$), momenta $\mathbf{p}_i = m_i \mathbf{v}_i$, and intrinsic angular momenta $\mathbf{j}_i = \mathbf{I}_i \boldsymbol{\omega}_i$, which obey the

equations of motion $\dot{\mathbf{p}}_i = \mathbf{F}_i$, $\dot{\mathbf{j}}_i = \boldsymbol{\tau}_i$, $\dot{\mathbf{r}}_i = \mathbf{p}_i / m_i$, and $\dot{\mathbf{e}}_i^{(\alpha)} = (\mathbf{I}_i^{-1} \mathbf{j}_i) \times \mathbf{e}_i^{(\alpha)}$. Here \mathbf{F}_i and $\boldsymbol{\tau}_i$ denote the total forces and torques acting on particle i . The time evolution of the N -particle distribution function $\mathcal{P}(\Gamma, t)$ with $\Gamma = \{\mathbf{r}_i, \mathbf{p}_i, \mathbf{e}_i^{(1,2)}, \mathbf{j}_i\}$ is described by a Fokker-Planck equation $\partial_t \mathcal{P} = L_{\text{FP}} \mathcal{P}$. We focus on the contributions of the deterministic tangential friction force, L_{ik}^{f} , and the corresponding stochastic force, L_{ik}^{fn} , to the Fokker-Planck operator L_{FP} :

$$L_{\text{FP}} = \sum_{i < k} (L_{ik}^{\text{f}} + L_{ik}^{\text{fn}}) + \text{other contributions} \quad (10)$$

The deterministic term accounts for the effect of the friction force and torque, Eqs. (7) and (8), and can be decomposed into

$$L_{ik}^{\text{f}} = (\partial_{\mathbf{p}_k} - \partial_{\mathbf{p}_i}) \mathbf{J}_{ik,\mathbf{p}}^{\text{f}} - (\partial_{\mathbf{j}_i} R_i + \partial_{\mathbf{j}_k} R_k) \mathbf{J}_{ik,\mathbf{j}}^{\text{f}} \quad (11)$$

with probability current operators

$$\begin{aligned} \mathbf{J}_{ik,\mathbf{p}}^{\text{f}} &= \frac{f(u_{ik}^\perp, r_{ik})}{u_{ik}^\perp} \left(\mathbf{P}(\hat{\mathbf{r}}_{ik}) \left(\frac{\mathbf{p}_k}{m_k} - \frac{\mathbf{p}_i}{m_i} \right) \right. \\ &\quad \left. + \hat{\mathbf{r}}_{ik} \times (\mathbf{I}_i^{-1} \mathbf{j}_i R_i + \mathbf{I}_k^{-1} \mathbf{j}_k R_k) \right), \end{aligned} \quad (12)$$

$$\begin{aligned} \mathbf{J}_{ik,\mathbf{j}}^{\text{f}} &= \frac{f(u_{ik}^\perp, r_{ik})}{u_{ik}^\perp} \left(\hat{\mathbf{r}}_{ik} \times \left(\frac{\mathbf{p}_k}{m_k} - \frac{\mathbf{p}_i}{m_i} \right) \right. \\ &\quad \left. - \mathbf{P}(\hat{\mathbf{r}}_{ik}) (\mathbf{I}_i^{-1} \mathbf{j}_i R_i + \mathbf{I}_k^{-1} \mathbf{j}_k R_k) \right). \end{aligned} \quad (13)$$

We assume that it is possible to construct stochastic forces and torques $\mathbf{F}_{ik}^{\text{fn}}$ and $\boldsymbol{\tau}_{ik}^{\text{fn}}$ such that the corresponding Fokker-Planck operator can be decomposed in the same manner,

$$L_{ik}^{\text{fn}} = (\partial_{\mathbf{p}_k} - \partial_{\mathbf{p}_i}) \mathbf{J}_{ik,\mathbf{p}}^{\text{fn}} - (\partial_{\mathbf{j}_i} R_i + \partial_{\mathbf{j}_k} R_k) \mathbf{J}_{ik,\mathbf{j}}^{\text{fn}} \quad (14)$$

such that

$$\left(\mathbf{J}_{ik,\mathbf{p}}^{\text{f}} + \mathbf{J}_{ik,\mathbf{p}}^{\text{fn}} \right) \mathcal{P}_{\text{B}} = 0 \quad (15)$$

$$\left(\mathbf{J}_{ik,\mathbf{j}}^{\text{f}} + \mathbf{J}_{ik,\mathbf{j}}^{\text{fn}} \right) \mathcal{P}_{\text{B}} = 0. \quad (16)$$

for the Boltzmann distribution

$$\mathcal{P}_{\text{B}}(\Gamma) \propto \exp \left[-\frac{1}{k_{\text{B}} T} \left(U(\{\mathbf{r}_i\}) + \sum_i \left(\frac{\mathbf{p}_i^2}{2m_i} + \frac{1}{2} \mathbf{j}_i \mathbf{I}_i^{-1} \mathbf{j}_i \right) \right) \right]. \quad (17)$$

In other words, we request that the Boltzmann distribution is not only the stationary solution of the equilibrium Fokker-Planck equation, but also, that all probability currents $\mathbf{J}_{\text{FP},ik,\mathbf{p}}^{\text{fn}} \mathcal{P}_{\text{B}}$ and $\mathbf{J}_{\text{FP},ik,\mathbf{j}}^{\text{fn}} \mathcal{P}_{\text{B}}$ vanish individually.

In general, the stochastic forces and torques will depend on the instantaneous momenta and angular momenta of particles and generate multiplicative noise. Hence the structure of the probability currents depends on the choice of stochastic calculus.²⁹ Here, we will discuss three popular choices: (i) the Itô calculus, which is commonly implemented in numerical simulations, (ii)

the Stratonovich calculus, which is commonly used in physical theories because it preserves the chain rule, (iii) the Hänggi-Klimontovich calculus^{30–32}. Loosely speaking, they differ in their definitions how to evaluate the integrand in discrete implementations of time integrals, $\int f(t) dt = \sum_i ((1-\theta)f_i + \theta f_{i+1})(t_{i+1} - t_i)$. The Itô calculus specifies $\theta = 0$, the Stratonovich calculus $\theta = 1/2$, and the Hänggi-Klimontovich calculus $\theta = 1$. We can account for all three possibilities by making the following Ansatz for the probability currents (see Section IV A):

$$\mathbf{J}_{ik,p}^{\text{fn}} = k_{\text{B}}T D(u_{ik}^{\perp}, r_{ik})^{\theta} \left(\mathbf{P}(\hat{\mathbf{r}}_{ik}) (\partial_{\mathbf{p}_k} - \partial_{\mathbf{p}_i}) + \hat{\mathbf{r}}_{ik} \times (\partial_{j_i} R_i + \partial_{j_k} R_k) \right) D(u_{ik}^{\perp}, r_{ik})^{1-\theta}, \quad (18)$$

$$\mathbf{J}_{ik,j}^{\text{fn}} = k_{\text{B}}T D(u_{ik}^{\perp}, r_{ik})^{\theta} \left(\hat{\mathbf{r}}_{ik} \times (\partial_{\mathbf{p}_k} - \partial_{\mathbf{p}_i}) - \mathbf{P}(\hat{\mathbf{r}}_{ik}) (\partial_{j_i} R_i + \partial_{j_k} R_k) \right) D(u_{ik}^{\perp}, r_{ik})^{1-\theta}. \quad (19)$$

Using the general identities $\mathbf{P}(\hat{\mathbf{r}})^2 \mathbf{u} = \mathbf{P}(\hat{\mathbf{r}}) \mathbf{u} = -\hat{\mathbf{r}} \times (\hat{\mathbf{r}} \times \mathbf{u})$, $\hat{\mathbf{r}} \times \mathbf{P}(\hat{\mathbf{r}}) \mathbf{u} = \mathbf{P}(\hat{\mathbf{r}}) (\hat{\mathbf{r}} \times \mathbf{u}) = \hat{\mathbf{r}} \times \mathbf{u}$, which are valid for all vectors \mathbf{u} , one can easily check that Eqs. (15) and (16) are fulfilled with this choice, if the function $D(u, r)$ obeys the differential equation

$$\nu k_{\text{B}}T \partial_u D(u, r) - D(u, r) u = -f(u, r) \quad (20)$$

with

$$\nu = (1-\theta) \left[\left(\frac{1}{m_i} + \frac{1}{m_k} \right) + (\mathbf{I}_i^{-1} R_i^2 + \mathbf{I}_k^{-1} R_k^2) \right]. \quad (21)$$

The solution of Eq. (20) is

$$D(u, r) = \frac{1}{k_{\text{B}}T\nu} \int_u^{\infty} du' f(u', r) e^{-(u'^2 - u^2)/2k_{\text{B}}T\nu} \quad (22)$$

for $\nu \neq 0$ (Itô and Stratonovich case) and

$$D(u, r) = k_{\text{B}}T f(u, r)/u \quad (23)$$

for $\nu = 0$ (Hänggi-Klimontovich case). We note that (22) reduces to (23) in the special case of additive noise with $f(u, r) \propto u$.

The probability currents (18) and (19) correspond to the following random force and torque terms in the stochastic differential equations of motion:

$$\mathbf{F}_{ik}^R = -\mathbf{F}_{ki}^R = \sqrt{D(u_{ik}^{\perp}, r_{ik})} \left[\mathbf{P}(\hat{\mathbf{r}}_{ik}) \boldsymbol{\xi}_{ik}^f - \hat{\mathbf{r}}_{ik} \times \mathbf{N}_{ik}^f \right], \quad (24)$$

$$\frac{\boldsymbol{\tau}_{ik}^R}{R_i} = \frac{\boldsymbol{\tau}_{ki}^R}{R_k} = \sqrt{D(u_{ik}^{\perp}, r_{ik})} \left[\hat{\mathbf{r}}_{ik} \times \boldsymbol{\xi}_{ik}^f + \mathbf{P}(e_{ik}) \mathbf{N}_{ik}^f \right], \quad (25)$$

where $\boldsymbol{\xi}_{ik}^f$ and \mathbf{N}_{ik}^f are three-dimensional Gaussian white noise vectors with correlations

$$\langle \boldsymbol{\xi}_{ik}^f(t) \boldsymbol{\xi}_{kl}^f(t') \rangle = k_{\text{B}}T \mathbf{1} (\delta_{ik} \delta_{jl} - \delta_{il} \delta_{jk}) \delta(t - t') \quad (26)$$

$$\langle \mathbf{N}_{ik}^f(t) \mathbf{N}_{kl}^f(t') \rangle = k_{\text{B}}T \mathbf{1} (\delta_{ik} \delta_{jl} + \delta_{il} \delta_{jk}) \delta(t - t'). \quad (27)$$

A derivation of these expressions is provided in the Section IV A.

4. Specific examples of friction types

We will now discuss three particularly interesting choices of amplitude functions $f(u, r)$. The first choice is the *linear friction* model:

$$f_l(u, r) = w(r) \gamma_f u \quad (28)$$

The integral (22) then simply gives

$$D_l(u, r) = w(r) \gamma_f \quad (29)$$

and the noise is additive as discussed above. In the linear case, the combined deterministic friction and stochastic forces can be seen as very complicated dissipative particle dynamics (DPD) thermostat³³, which extends a transverse DPD thermostat³⁴ by terms that couple the rotation and translation of particles.

The second interesting choice is the *constant friction* or *Coulomb friction* model:⁴

$$f_c(u, r) = w(r) \kappa_f \quad (30)$$

It results in multiplicative noise, with the squared amplitude having the form of a complementary error function, which can be evaluated very efficiently in numerical applications:

$$D_c(u, r) = \frac{w(r) \kappa_f \sqrt{\pi}}{\sqrt{2k_{\text{B}}T\nu}} e^{\frac{u^2}{2k_{\text{B}}T\nu}} \text{Erfc}\left(\frac{u}{\sqrt{2k_{\text{B}}T\nu}}\right) \quad (31)$$

This model works well in practice as we shall show below, but it has the conceptual problem that the friction force does not have a well-defined limit at $u \rightarrow 0^{\pm}$, and may rapidly oscillate between finite positive and negative forces for small tangential velocities.

The third example, the *Coulomb-Newton friction* model avoids this problem and is popular in granular matter models⁴:

$$f_{\text{CN}}(u, r) = \min[\gamma_f u, w(r) \kappa_f] \quad (32)$$

In this case, the function $D_{\text{CN}}(u, r)$ is given by

$$D_{\text{CN}}(u, r) = \begin{cases} \frac{w(r) \kappa_f \sqrt{\pi}}{\sqrt{2k_{\text{B}}T\nu}} e^{\frac{u^2}{2k_{\text{B}}T\nu}} \text{Erfc}\left(\frac{u}{\sqrt{2k_{\text{B}}T\nu}}\right) & : u \geq \frac{w(r) \kappa_f}{\gamma_f} \\ \gamma_f \left(1 - e^{\left(u^2 - \left(\frac{w(r) \kappa_f}{\gamma_f}\right)^2\right)/2k_{\text{B}}T\nu} \right) & \\ + \frac{w(r) \kappa_f \sqrt{\pi}}{\sqrt{2k_{\text{B}}T\nu}} e^{\frac{u^2}{2k_{\text{B}}T\nu}} \text{Erfc}\left(\frac{w(r) \kappa_f / \gamma_f}{\sqrt{2k_{\text{B}}T\nu}}\right) & : u < \frac{w(r) \kappa_f}{\gamma_f} \end{cases} \quad (33)$$

In all three examples, $w(r)$ is a smooth function of the center-to-center distance between the particles i, k , which ensures that the friction vanishes if the particles are far apart. In the classical Coulomb friction model, the tangential friction force is assumed to be proportional to the normal (repulsive) conservative force between the particles. In the applications shown below, we will consider particles that interact via a purely repulsive Weeks-Chandler-Anderson (WCA) potential³⁵,

$$U_{\text{WCA}}(r) = \begin{cases} 4\epsilon \left[\left(\frac{\sigma}{r}\right)^{12} - \left(\frac{\sigma}{r}\right)^6 \right] + \epsilon & , r \leq \sqrt[6]{2}\sigma \\ 0 & , r > \sqrt[6]{2}\sigma. \end{cases} \quad (34)$$

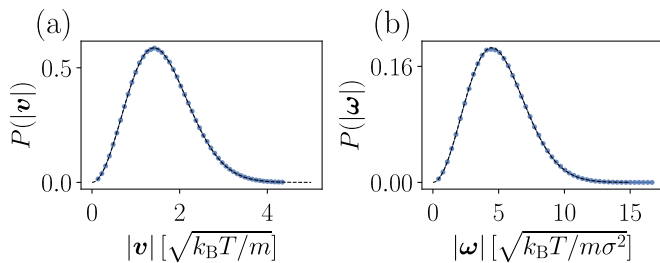


FIG. 2. Velocity (a) and angular velocity (b) distribution in a three-dimensional system of passive colloids interacting with repulsive WCA interactions and contact forces according to the Coulomb-Newton friction model (Eq. (32)) with noise, using $\gamma_f = 3 \cdot \sqrt{mk_B T} / \sigma$, $\kappa_f = 5$. Blue symbols show simulation results, lines show the Maxwell-Boltzmann distribution.

Therefore, adopting the Coulomb friction Ansatz, we will choose $w(r) = -dU_{\text{WCA}}(r)/dr$.

To validate our approach, we have performed three-dimensional simulations of systems of identical passive colloids interacting with repulsive WCA interactions and frictional contact interactions of the Coulomb-Newton type (with $R = \sigma/2$ and $k_B T = \epsilon$). No additional thermostat is applied. We use a simple Euler-forward scheme to integrate over stochastic forces, corresponding to an implementation of Itô calculus. Fig. 2 shows the resulting distributions of the velocities and angular velocities of particles. They are in perfect agreement with the Maxwell-Boltzmann distribution.

B. Application examples

In the following, we investigate the effect of frictional contact forces in three different systems: First, in Section II B 1, we simulate simple passive fluids to demonstrate the thermodynamic inconsistencies that arise if only the deterministic frictional contact forces are included in a model. Second, in Section II B 2, we consider pressure-driven Poiseuille flows in a slit channel and investigate the coupling of velocity and angular velocity gradients due to frictional contacts in such channels. Furthermore, we use the flow profiles to determine the dynamic viscosity arising from frictional contact interactions. Last, in Section II B 3, we study the influence of frictional contacts on motility-induced phase separation (MIPS) in systems of active particles.

All particles have identical masses m , radii $R = \sigma/2$, and moments of inertia $\mathbf{I} = \frac{2}{5}mR^2\mathbf{1}$, interact with WCA interactions (Eq. (34)), and may be coupled to a solvent

bath. The basic equations of motion read

$$m\dot{\mathbf{v}}_i = \mathbf{F}_i^{\text{ne}} - \gamma\mathbf{v}_i + \boldsymbol{\xi}_i^{\text{s}} + \sum_{k \neq i} (-\nabla_i U_{\text{WCA}}(r_{ik}) + \mathbf{F}_{ik}^{\text{f}} + \mathbf{F}_{ik}^{\text{fn}}) \quad (35)$$

$$\frac{d}{dt}(\mathbf{I}\boldsymbol{\omega}_i) = -\gamma_R\boldsymbol{\omega}_i + \mathbf{N}_i^{\text{s}} + \sum_{k \neq i} (\boldsymbol{\tau}_{ik}^{\text{f}} + \boldsymbol{\tau}_{ik}^{\text{fn}}) \quad (36)$$

$$\dot{\mathbf{e}}_i^{(\alpha)} = \boldsymbol{\omega}_i \times \mathbf{e}_i^{(\alpha)} \quad \text{for } \alpha = 1, 2 \quad (37)$$

$$\dot{\mathbf{r}}_i = \mathbf{v}_i \quad (38)$$

where γ and γ_R are translational and rotational friction coefficients describing the interaction with the solvent, and the forces $\boldsymbol{\xi}_i^{\text{s}}$ and torques \mathbf{N}_i^{s} are uncorrelated Gaussian white noise terms with zero mean and variance

$$\langle \boldsymbol{\xi}_i^{\text{s}}(t) \boldsymbol{\xi}_k^{\text{s}}(t') \rangle = 2k_B T \gamma \mathbf{1} \delta_{ik} \delta(t - t') \quad (39)$$

$$\langle \mathbf{N}_i^{\text{s}}(t) \mathbf{N}_k^{\text{s}}(t') \rangle = 2k_B T \gamma_R \mathbf{1} \delta_{ik} \delta(t - t'), \quad (40)$$

The forces $\mathbf{F}_{ik}^{\text{f/R}}$ and torques $\boldsymbol{\tau}_{ik}^{\text{f/R}}$ model interparticle frictional contacts and as described in the previous section. Additional forces \mathbf{F}_i^{ne} may drive the system out of equilibrium. All densities are expressed by the area fraction $\rho_{\text{area}} = \pi N R^2 / A$ and by the volume fraction $\rho_{\text{volume}} = 4\pi N R^3 / 3V$, where N is the number of particles, and A , V are the area and the volume. In two-dimensional systems, the position of the particles is restricted to a plane.

All quantities will be given in units of the length σ , the thermal energy $k_B T$, and a “natural” time unit t_0 .

1. Thermodynamic consistency in models with frictional contact interactions

In Section II A, we have shown that dissipative frictional forces necessarily reduce the kinetic energy of colliding particles, but combined dissipative and stochastic frictional forces constitute a valid thermostat in simulations of passive colloidal systems (see Fig. 2). When considering systems of particles in an implicit solvent as in Eqs. (35) and (36), one might be tempted to omit the stochastic force and torque terms, $\mathbf{F}_{ik}^{\text{R}}$ and $\boldsymbol{\tau}_{ik}^{\text{R}}$, assuming that the coupling to a solvent bath (i.e., the corresponding Langevin thermostat) is sufficient to guarantee sampling of a canonical ensemble in the absence of nonequilibrium forces \mathbf{F}_i^{ne} . In the following, we will demonstrate that this assumption is not correct, and that the stochastic frictional contact terms must necessarily be included to avoid thermodynamic inconsistencies.

For this purpose, we have investigated two and three-dimensional systems of passive particles with frictional contact interactions, which are coupled to a solvent as described above. The nonequilibrium forces were set to zero, $\mathbf{F}_i^{\text{ne}} = \boldsymbol{\tau}_i^{\text{ne}} = 0$. The area fraction of the two-dimensional system was chosen $\rho_{\text{area}} = 0.6$ and the volume fraction of the three-dimensional system $\rho_{\text{volume}} =$

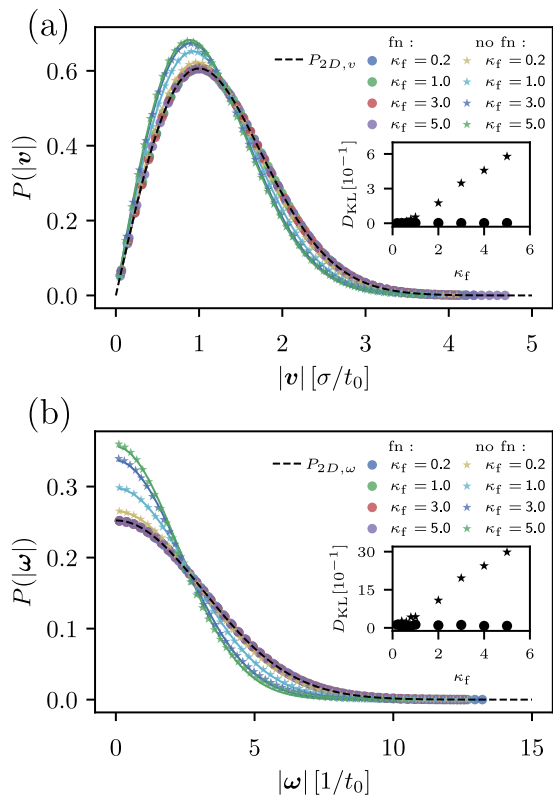


FIG. 3. (a) Velocity histograms and (b) angular velocity histograms for a two dimensional passive colloid system with frictional contact interactions according to the constant friction model, Eq. (30), for different friction constants κ_f as indicated. Stars show data from simulations without stochastic contact friction terms, circles data for the full model. Solid colored lines are fits to appropriate Maxwell-Boltzmann distribution with fitted effective temperature, T_{eff} , black solid line gives the theoretical expectation for $k_B T_{\text{eff}} = k_B T$. The inset shows the corresponding Kullback-Leibler divergence between the distribution measured in simulations and the fitted Maxwell-Boltzmann distribution.

0.3. All systems contain $N = 10000$ particles with periodic boundary conditions in all directions. We performed simulations for the friction types linear, constant and Coulomb-Newton. Each type was simulated twice, once without stochastic friction \mathbf{F}_{ik}^R and torques $\boldsymbol{\tau}_{ik}^R$ and once including them. The systems were equilibrated over a time $20t_0$ using a time step of $\Delta t = 0.001t_0$ for the linear and Coulomb-Newton friction model and $\Delta t = 0.0001t_0$ for the constant friction model. The data were then collected over a simulation time period of $200t_0$. The distributions of velocities and angular velocities were then compared to the theoretically expected Maxwell-Boltzmann distributions at the solvent temperature $k_B T$.

Fig. 3 depicts such a comparison exemplarily for a two-dimensional system with frictional contacts according to the constant friction model and different values of κ_f . Corresponding figures for other types of friction and in three dimensions are provided in supplemental informa-

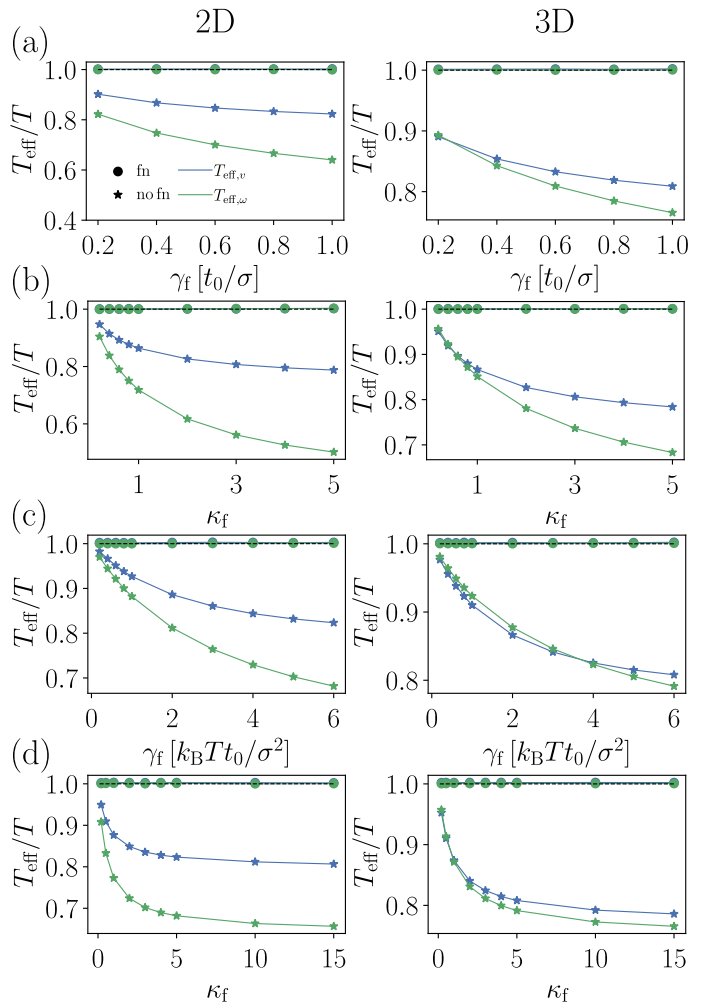


FIG. 4. T_{eff} Effective kinetic temperatures obtained by fitting velocity (green) and angular velocity (blue) histograms to the corresponding Maxwell-Boltzmann distributions from simulations without (stars) and with (circles) stochastic contact friction terms in two dimensional (left) and three dimensional (right) systems and for different friction types: (a) linear friction model (b) constant friction model, (c,d) Coulomb-Newton friction model with (c) fixed $\kappa_f = 5$ and varying γ_f , and (d) fixed $\gamma_f = 6 k_B T t_0 / \sigma^2$ and varying κ_f .

tion (Supplementary Fig. S2 and Fig. S3). When omitting the stochastic contact forces and torques in the simulations (star symbols), the velocity and angular velocity distributions clearly deviate from the theoretically expected Maxwell-Boltzmann distribution $P_{2d,v}$ and $P_{2d,\omega}$, which is shown as dashed black line. However, when the stochastic contact terms are included, the simulation data (circles) coincide with the expectation.

One might argue that the main effect of omitting the stochastic contact terms is to reduce the kinetic temperature of the particles, but that the system might still adopt an “equilibrium” state corresponding to such a reduced temperature. However, a closer look at the data shows that this is not the case. First, we can determine the

“effective” temperature T_{eff} by fitting the velocity and angular velocity histograms to the Maxwell-Boltzmann distribution, using T_{eff} as fit parameter. The result is shown in Fig. 4 for two- and three-dimensional systems, three different types of contact friction, and varying friction parameters. Not surprisingly, the effective temperature decreases with increasing friction parameters. More importantly, however, the effective kinetic temperature obtained from the velocity histogram and the angular velocity histogram differ from each other. This clearly indicates that the system cannot be mapped to an equilibrium system.

A second, more subtle nonequilibrium signature is that the shape of the distribution also differs from the expected Maxwell-Boltzmann shape. To quantify this, we have calculated the Kullback-Leibler divergence, D_{KL} , between the real (simulated) histograms and the fitted histograms with shifted effective temperature:

$$D_{\text{KL}}(P_{\text{sim}}(\mathbf{x})||P_{\text{fit}}(\mathbf{x})) = \int d\mathbf{x} P_{\text{sim}}(\mathbf{x}) \ln \left(\frac{P_{\text{sim}}(\mathbf{x})}{P_{\text{fit}}(\mathbf{x})} \right), \quad (41)$$

where \mathbf{x} stands for \mathbf{v} or $\boldsymbol{\omega}$, $P_{\text{sim}}(\mathbf{x})$ is the distribution from simulation, and $P_{\text{fit}}(\mathbf{x})$ the fitted distribution. The results for the constant friction model are shown in the insets of Fig. 3. If the stochastic contact terms are omitted in the simulation, the Kullback-Leibler divergence deviates from zero for large friction parameters, indicating that the shape of the distribution from the simulations deviates from the fitted Maxwell-Boltzmann distribution. If the stochastic terms are included, the Kullback-Leibler divergence is zero, hence the simulations produce the correct distribution functions.

2. Pressure-driven flows

Next we study the dynamic properties of fluids of repulsive particles with frictional contact interactions that are subject to an external bulk force in a slit channel. In this case, the particles are not coupled to a solvent, and the parameters γ and γ_R in Eqs. (35, 36) are set to zero. The nonequilibrium forces are set to $\mathbf{F}_i^{\text{ne}} \equiv F \mathbf{e}_x$, i.e., all particles are subject to a constant bulk force in the x direction. Such a setup is commonly used to mimic pressure-driven flows³⁶ in a pressure gradient $dP/dx = -F n$, where n is the local number density of particles ($n = N/V$ in homogeneous systems). The particles are confined by two identical walls, consisting of a layer of immobilized particles j with diameter σ and z -coordinates

$$y_j = \pm 8.5847\sigma + \delta_w \zeta_j, \quad (42)$$

which are arranged on a square lattice with lattice constant $a = \sigma$ in the (xz) -plane. In Eq. 42, ζ_j denotes uncorrelated random numbers that are drawn from a Gaussian distribution with mean zero and variance 1, and the parameter $\delta_w > 0$ allows to tune the degree

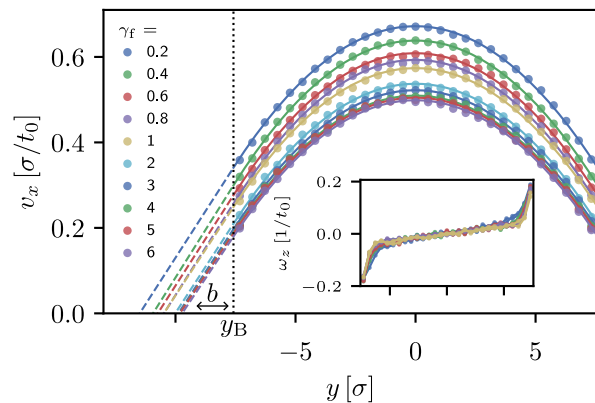


FIG. 5. Examples of velocity profiles for fluids with frictional contact interactions of the Coulomb-Newton type with parameter $\kappa_f = 5$ and different values of γ_f as indicated, which are confined between walls with roughness parameter $\delta_w = 0$ (see text) and subject to a bulk force $F = 0.01 k_B T / \sigma$. Solid lines show fit to a parabolic profile. Inset shows corresponding profiles of the z -component of the angular velocity.

of surface roughness. For technical reasons, the random numbers are the same on both sides of the slab. All particles, mobile and immobile, interact via repulsive WCA interactions and frictional contact interactions of the Coulomb-Newton type (Eq. 32). We considered systems of 10000 particles at volume fraction $\rho = 0.15$ in a simulation box with accessible volume $V = (151.694 \times 15.1694 \times 15.1694) \sigma^3$, and periodic boundary conditions in all directions. The time step in the simulations was $\Delta t = 0.001 t_0$. After initialization, each system was simulated over a time of $500 t_0$, which was sufficient to reach a stationary state (Supplementary Fig. S4). Data were then collected over a simulation time period of $6000 t_0$. In the following, we will show data obtained for bulk forces $F = 0.01 k_B T / \sigma$. We have also simulated systems at $F = 0.02 k_B T / \sigma$ and verified that the velocity and angular velocity profiles are proportional to F as expected in the linear regime.

Fig. 5 (main figure) shows examples of resulting velocity profiles for different thermostat parameters γ_f at roughness parameter $\delta_w = 0$. They have the parabolic shape expected for Poiseuille flow of Newtonian fluids, if one allows for substantial slip at the surface. Compared to regular DPD simulations of Poiseuille flow, in our system, slip is facilitated by the possibility that particles roll off on the surface without dissipating energy due to friction. This rolling involves a collective rotational motion to the particles, which however quickly decreases further away from the surface. More generally, the inset of Fig. 5 (main figure) demonstrates that shear in the velocity profiles ($dv_x/dv_y \neq 0$) induces rotational motion of particles in the fluid.

Fitting the velocity profiles in Fig. 5 to the prediction of the Stokes equation for a fluid with volume fraction ρ_{volume} and partial slip boundary conditions

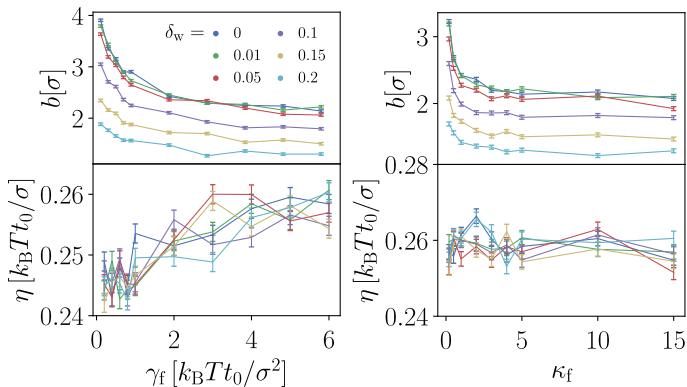


FIG. 6. Slip length b (top) and dynamic viscosity η (bottom) as obtained from parametric fits to Poiseuille flow simulation profiles as in Fig. 5 of fluids with frictional contact interactions of the Coulomb-Newton type in slit geometry. The results are shown for various values of the surface roughness parameter δ_w as functions of the friction parameter γ_f with fixed $\kappa_f = 5$ (left), and κ_f with fixed $\gamma_f = 6 k_B T t_0 / \sigma^2$ (right). Error bars represent the one standard deviation uncertainties of the fitted parameters.

$$(v_x(y_B)/v'_x(y_B) = b),$$

$$v_x(y) = -\frac{3\rho_{\text{volume}}}{\pi\eta} F(y^2 - y_B^2) + \frac{6\rho_{\text{volume}}}{\pi\eta} F y_B b, \quad (43)$$

we can extract the dynamic viscosity η and a parameter $\alpha = y_B b + y_B^2/2$ which depends on the slip length b and the hydrodynamic boundary position y_B . Unfortunately, y_B and b are interdependent fit parameters and separate simulations of Couette flows would be necessary to disentangle them³⁷. Here we will simply assume that the hydrodynamic boundary coincides with the physical boundary, i.e., the accessible y -values for particles, $y_B = \pm 7.5847\sigma$, which is compatible to findings from previous studies of simple fluids at hard walls^{37,38}.

The results of such fits are shown in Fig. 6. Interestingly, the dynamic shear viscosity of the fluid only slightly increases with the friction parameter γ_f and is independent of the parameter κ_f , indicating that, at this volume fraction, the shear viscosity is basically determined by the conservative interactions between the particles. In contrast, the contact friction has a strong influence on the surface slip: The stronger the contact friction interactions, the smaller the slip length. Nevertheless, it seems difficult to achieve zero slip length in this system due to the possibility that particles can roll off at the surface. The slip length is roughly independent of the roughness parameter δ_w up to $\delta_w = 0.05$ and then decreases steadily as δ_w is increased further.

Even though our results so far suggest that the flow profiles can be described by the Stokes equation, the relatively strong coupling to angular rotation motion suggests that nonlinear rheological effects might be important in fluids involving frictional contact interactions. Unfortunately, increasing the driving force F and pushing it into the nonlinear regime mainly has the effect of

increasing the slip length, such that the flow profile becomes plug like (data not shown). In order to avoid this effect and investigate the coupling between shear rate and rotational motion of particles at higher shear rates, we have used an artificial simulation setup which is popular in rheological simulation studies of complex fluids^{39,40}: We apply periodic boundary conditions in *all* directions, but split the simulation box in half in the y direction and impose opposing bulk forces in both halves: $\mathbf{F}_i^{\text{ne}} = F \mathbf{e}_x$ for $y_i > 0$, and $\mathbf{F}_i^{\text{ne}} = -F \mathbf{e}_x$ for $y_i < 0$. According to the Stokes equation, this should result in a sequence of two parabolic flow profiles in opposite directions. In our simulations, we found that, instead, vortices developed in the high shear regions at higher forces bulk forces, which eventually destroyed the stationary Poiseuille-like flow profiles. An example for $F = 0.5 k_B T / \sigma$ is provided in Supplementary Movie 1. The formation of these vortices was prevented in the presence of solid walls. Nevertheless, our results suggest that the linear response regime in fluids with frictional contact interactions is small and that their dynamic behavior might often be dominated by nonlinear effects.

3. Active particles and motility-induced phase separation

As a final example, we consider the effect of frictional contact interactions on structure formation in systems of active particles. Specifically, we focus on the phenomenon of motility-induced phase separation (MIPS)⁴¹, which has been observed both in systems of active Brownian particles (ABPs) and active Langevin particles (ALPs). ALPs follow the equations of motion (Eqs. 35-38) with effective active force $\mathbf{F}_i^{\text{ne}} = F_0 \mathbf{e}^{(1)}$ (and originally without frictional contact terms)⁴². ABPs obey the same equations of motion as ALPs in the overdamped limit (Eqs. 35-38 with $m \rightarrow 0$ and $\mathbf{I} \rightarrow 0$). In a certain parameter range, the active force can induce phase separation between coexisting dense and dilute regimes even in the absence of attractive conservative forces between particles. The reason is, loosely speaking, that particles which happen to be pushed against each other by the active force remain stuck to each other for some time before they reorient. If other particles collide with the stuck particle assembly before the particles reorient the clusters tend to grow until the system is phase separated. Roughly, this happens at sufficiently high active particle speeds and densities, such that the collision rate is higher than the reorientation rate. Frictional contact forces can enhance particle aggregation, as they force the particles to rotate in the same direction, causing them to stick together even longer. This effect has recently been reported for systems of ABPs by Nie et al.²³ in a model that accounted for dissipative friction contact forces similar to the Coulomb-Newton type and which is also well-known in the granular community⁵. The model by Nie et al. did not include corresponding stochastic terms with thermodynamically consistent coupling of translational

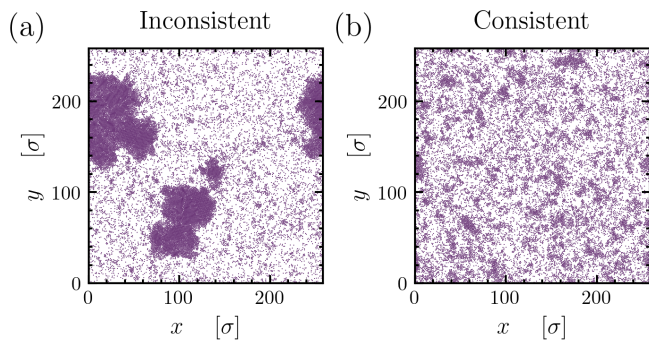


FIG. 7. Snapshots of ALP simulations of 20000 Particles after a sufficient equilibration period with Coulomb-Newton friction. (a) Thermodynamically inconsistent treatment and (b) thermodynamically consistent treatment of the frictional contacts. In the thermodynamically consistent treatment of frictional contacts, no MIPS occurs, whereas on the left MIPS can be seen. The parameters of the simulations are marked with a red circle in Fig. 8.

and rotational noise.

In our simulations we study two-dimensional systems of $N = 20,000$ ALPs with model parameters as specified earlier (beginning of Section II B), which were chosen in accordance to our previous work on MIPS where we know the parameter regime of the MIPS region⁴³. In particular, the mass is set to be $m = 0.05 k_B T (t_R/\sigma)^2$ which is still in the underdamped regime as compared to the overdamped system Nie et al. studied²³. We include frictional contact interactions of the Coulomb-Newton type with parameters $\gamma_f = 1 \cdot k_B T t_R / \sigma^2$ and $\kappa_f = 1$. The simulation time step was $\Delta t = 10^{-5} \cdot t_R$, and periodic boundary conditions were applied in all directions. Neglecting the thermodynamic correction of the frictional contacts, can cause the collective behavior to vary significantly. This can be seen in Fig. 7, where the simulation with thermodynamically inconsistent frictional contacts leads to MIPS, whereas the simulation of the consistent treatment shows no MIPS. To study the effect of the thermodynamically consistent treatment more systematically, we simulated a MIPS phase diagram for the different models, no frictional contacts, with Coulomb-Newton friction with and without frictional noise. MIPS was identified using AMEP⁴⁴ by computing the local density on a uniform grid. A bimodal distribution in the resulting density histogram indicates phase separation.

The resulting non-equilibrium MIPS phase diagrams for systems with and without frictional interactions are shown in Fig. 8. As reported by Nie et al.²³ for ABPs, the contact friction forces significantly expand the regime in which MIPS is observed. This can also be seen in the case of the inertial ALPs we investigated. More importantly, the comparison between the thermodynamically consistent case (with frictional noise) and the thermodynamically inconsistent case (no frictional noise) shows a notable difference in the morphology of the MIPS phase diagram. This shows that, neglecting rotational noise,

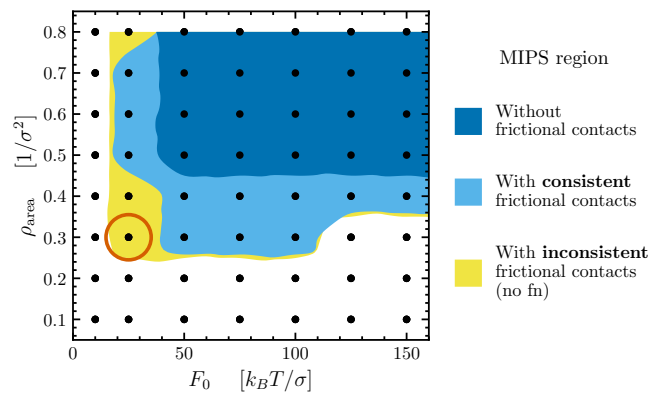


FIG. 8. MIPS regime in two-dimensional systems of ALPs without frictional contacts (dark blue), with thermodynamically incorrect frictional contacts (yellow) as well as correct frictional contacts (light blue) in the space of active force F_0 versus area fraction (number density) ρ_{area} . The black dots are the locations of simulations and the colored regions are from estimated MIPS transitions extracted from the simulation data. The red circle marks the simulation parameters of the simulation snapshots in Fig. 7. See text for further explanation.

despite altering the equilibrium distribution of colloidal particles only relatively mildly, can lead to a completely wrong prediction for the collective behavior of a non-equilibrium many particle system in certain parameter regimes.

III. CONCLUSION

In sum, we have constructed a thermodynamically consistent way of modelling thermal fluctuations in particle models with frictional contact interactions. Our approach is based on the construction of appropriate Fokker-Planck equations for such systems under the constraint that the stationary solution for equilibrium systems should be the Boltzmann distribution function. Importantly, it shows that coupled frictional forces and torques arising from frictional contacts must necessarily be accompanied by stochastic forces and torques that are coupled in a structurally similar manner. We have demonstrated that neglecting such stochastic terms in equilibrium simulations results in stationary distribution that differ from the Boltzmann distribution, both regarding effective temperature and shapes of the distribution.

We have considered a general form of frictional contact interactions, which is inspired by models for granular matter. In general, the resulting stochastic terms depend on the velocities and angular velocities of particles and are therefore instances of multiplicative noise. Hence, we have separately considered three popular choices of stochastic calculus, Itô, Stratonovich, and Hänggi-Klimontovich, and we have provided explicit expressions for the stochastic Langevin noise terms for all three

choices. Then we have validated the approach with simulations based on the Itô calculus and presented applications to Poiseuille flow and active particles undergoing motility induced phase separation.

In the case of Poiseuille flow, we have seen that frictional contacts lead to a coupling of rotational and translational degrees of freedom, which may lead to nonlinear effects already at low driving forces. In the case of MIPS, we have recovered the result of a previous study²³ that frictional contacts encrease the width of the phase separated region. We anticipate that the coupling of rotational and translational noise might be relevant in active chiral matter and unveil new mechanisms of pattern formation.

In future work, it will be interesting to extend our approach to the overdamped case. Unfortunately, taking the limit $m \rightarrow 0$ and $\mathbf{I} \rightarrow 0$ is tricky in the presence of frictional contacts, as – depending on the model – either the deterministic friction terms, or the corresponding stochastic terms, or both, depend on the velocities and angular velocities of the particles. Therefore, a separate treatment will be necessary. However, the present study suggests that also in underdamped models, e.g., for active Brownian particles, the coupling of rotational and translational stochastic terms will be crucial to achieve thermodynamic consistency. Studying this will be subject of future work.

IV. METHODS

A. Theory: Relation between Langevin equation and the Fokker-Planck equation

We recall the general relation between the Langevin equation and the Fokker-Planck equation for systems with many variables²⁹. We consider a system of stochastic differential equations for a vector of N variables, $\mathbf{x} = \{x_i\}$ with the Langevin equation

$$\dot{\mathbf{x}} = \boldsymbol{\mu}(\mathbf{x}, t) + \boldsymbol{\sigma}(\mathbf{x}, t) \boldsymbol{\eta}(t), \quad (44)$$

where $\boldsymbol{\eta}(t)$ is an uncorrelated Gaussian white noise vector with fluctuations

$$\langle \eta_\alpha(t) \eta_\beta(t') \rangle = \delta_{\alpha\beta} \delta(t - t'). \quad (45)$$

Then the corresponding Fokker-Planck equation for the distribution function $P(\mathbf{x}, t)$ is

$$\partial_t \mathcal{P} = - \sum_{\alpha} \partial_{\alpha} \mu_{\alpha}(\mathbf{x}) \mathcal{P} - \sum_{\alpha} J_{\alpha}^{\text{fn}} \mathcal{P} \quad (46)$$

with^{29,45}

$$J_{\alpha}^{\text{fn}} = - \frac{1}{2} \sum_{\beta, \gamma} \partial_{\beta} \sigma_{\alpha\gamma}(\mathbf{x}, t) \sigma_{\beta\gamma}(\mathbf{x}, t) \quad (47)$$

in the Itô calculus,

$$J_{\alpha}^{\text{fn}} = - \frac{1}{2} \sum_{\beta, \gamma} \sigma_{\alpha\gamma}(\mathbf{x}, t) \partial_{\beta} \sigma_{\beta\gamma}(\mathbf{x}, t) \quad (48)$$

in the Stratonovich calculus, and

$$J_{\alpha}^{\text{fn}} = - \frac{1}{2} \sum_{\beta, \gamma} \sigma_{\alpha\gamma}(\mathbf{x}, t) \sigma_{\beta\gamma}(\mathbf{x}, t) \partial_{\beta} \quad (49)$$

in the Hänggi-Klimontovich calculus. If $\boldsymbol{\sigma}$ does not depend on \mathbf{x} (additive noise), then all formalisms give the same Fokker-Planck equation.

With these general relations in mind, our task is to translate the Fokker-Planck probability operators $\mathbf{J}_{ik, \mathbf{p}}^{\text{fn}}$ and $\mathbf{J}_{ik, \mathbf{j}}^{\text{fn}}$, Eqs. (18) and (19), into stochastic force and torque terms in the equations of motion of the particles i and k . In the notation of Eqs. (44) - (49), the sum $[\mathbf{J}_{ik, \mathbf{p}}^{\text{fn}} + \mathbf{J}_{ik, \mathbf{j}}^{\text{fn}}]_{\alpha}$ corresponds to terms $-\frac{1}{2} \sum_{\beta, \gamma} \partial_{\beta} \sigma_{\alpha\gamma}^{(ik)} \sigma_{\beta\gamma}^{(ik)}$, $-\frac{1}{2} \sum_{\beta, \gamma} \sigma_{\alpha\gamma}^{(ik)} \partial_{\beta} \sigma_{\beta\gamma}^{(ik)}$, or $-\frac{1}{2} \sum_{\beta, \gamma} \sigma_{\alpha\gamma}^{(ik)} \sigma_{\beta\gamma}^{(ik)} \partial_{\beta}$, depending on the calculus, where the indices α, β, γ can take 12 values corresponding to the components of the variables $\mathbf{p}_i, \mathbf{p}_k, \mathbf{j}_i, \mathbf{j}_k$. We can decompose the matrices $\boldsymbol{\sigma}^{(ik)}$ as $\boldsymbol{\sigma}^{(ik)} = \sqrt{k_{\text{B}}T} D(u_{ik}^{\perp}, r_{ik}) \hat{\boldsymbol{\sigma}}^{(ik)}$ with reduced matrices $\hat{\boldsymbol{\sigma}}(\hat{\mathbf{r}}_{ik})$ that are independent of $\mathbf{p}_i, \mathbf{p}_k, \mathbf{j}_i, \mathbf{j}_k$ and satisfy

$$\frac{1}{2} \hat{\boldsymbol{\sigma}} \hat{\boldsymbol{\sigma}}^T = \left(\begin{array}{cc|cc} \mathbf{P}(\hat{\mathbf{r}}_{ik}) & -\mathbf{P}(\hat{\mathbf{r}}_{ik}) & -R_i \mathbf{A}(\hat{\mathbf{r}}_{ik}) & -R_k \mathbf{A}(\hat{\mathbf{r}}_{ik}) \\ -\mathbf{P}(\hat{\mathbf{r}}_{ik}) & \mathbf{P}(\hat{\mathbf{r}}_{ik}) & R_i \mathbf{A}(\hat{\mathbf{r}}_{ik}) & R_k \mathbf{A}(\hat{\mathbf{r}}_{ik}) \\ \hline R_i \mathbf{A}(\hat{\mathbf{r}}_{ik}) & -R_i \mathbf{A}(\hat{\mathbf{r}}_{ik}) & R_i^2 \mathbf{P}(\hat{\mathbf{r}}_{ik}) & R_i R_k \mathbf{P}(\hat{\mathbf{r}}_{ik}) \\ R_k \mathbf{A}(\hat{\mathbf{r}}_{ik}) & -R_k \mathbf{A}(\hat{\mathbf{r}}_{ik}) & R_i R_k \mathbf{P}(\hat{\mathbf{r}}_{ik}) & R_k^2 \mathbf{P}(\hat{\mathbf{r}}_{ik}) \end{array} \right).$$

Here $\mathbf{A}(\hat{\mathbf{r}}_{ik})$ is defined as the antisymmetric matrix with $\mathbf{A}(\hat{\mathbf{r}}_{ik}) \mathbf{a} = \hat{\mathbf{r}}_{ij} \times \mathbf{a}$ for all \mathbf{a} . One possible solution for $\hat{\boldsymbol{\sigma}}$ is

$$\hat{\boldsymbol{\sigma}} = \left(\begin{array}{cc|cc} \mathbf{P}(\hat{\mathbf{r}}_{ik}) & 0 & -\mathbf{A}(\hat{\mathbf{r}}_{ik}) & 0 \\ -\mathbf{P}(\hat{\mathbf{r}}_{ik}) & 0 & \mathbf{A}(\hat{\mathbf{r}}_{ik}) & 0 \\ \hline R_i \mathbf{A}(\hat{\mathbf{r}}_{ik}) & 0 & R_i \mathbf{P}(\hat{\mathbf{r}}_{ik}) & 0 \\ R_k \mathbf{A}(\hat{\mathbf{r}}_{ik}) & 0 & R_k \mathbf{P}(\hat{\mathbf{r}}_{ik}) & 0 \end{array} \right).$$

This can be checked using the relations

$$\begin{aligned} \mathbf{P}(\hat{\mathbf{r}}_{ik}) \mathbf{P}(\hat{\mathbf{r}}_{ik})^T &= \mathbf{A}(\hat{\mathbf{r}}_{ik}) \mathbf{A}(\hat{\mathbf{r}}_{ik})^T = \mathbf{P}(\hat{\mathbf{r}}_{ik}) \\ \mathbf{A}(\hat{\mathbf{r}}_{ik}) \mathbf{P}(\hat{\mathbf{r}}_{ik})^T &= -\mathbf{P}(\hat{\mathbf{r}}_{ik}) \mathbf{A}(\hat{\mathbf{r}}_{ik})^T = \mathbf{A}(\hat{\mathbf{r}}_{ik}). \end{aligned}$$

With this choice of $\hat{\boldsymbol{\sigma}}$, half of the Gaussian random variables η_i actually do not enter the Langevin equations of motion and can be omitted. We denote the other half as $\boldsymbol{\xi}_{ij}^{\text{f}} = -\boldsymbol{\xi}_{ji}^{\text{f}}$ and $\mathbf{N}_{ij}^{\text{f}} = \mathbf{N}_{ji}^{\text{f}}$ and require them to be three-dimensional Gaussian white noise vectors with correlations

$$\begin{aligned} \langle \xi_{ij}^{\text{f}}(t) \xi_{kl}^{\text{f}}(t') \rangle &= k_{\text{B}}T \mathbf{1} (\delta_{ik} \delta_{jl} - \delta_{il} \delta_{jk}) \delta(t - t') \\ \langle \mathbf{N}_{ij}^{\text{f}}(t) \mathbf{N}_{kl}^{\text{f}}(t') \rangle &= k_{\text{B}}T \mathbf{1} (\delta_{ik} \delta_{jl} + \delta_{il} \delta_{jk}) \delta(t - t'). \end{aligned}$$

Then we can rewrite our random force and torque terms in the form of Eqs. (24) and (25).

B. Simulation parameters and units

The natural time unit t_0 is given by the inertial time unit $t_0 = \sqrt{m\sigma^2/k_{\text{B}}T}$ in Sections II B 1 and II B 2, and by the diffusive time unit $t_{\text{R}} = \gamma_{\text{R}}/k_{\text{B}}T$ in Section II B 3.

In Sections **II B 1** and **II B 2**, we choose $\gamma_R = \pi k_B T t_0$, $\gamma = \frac{3}{4R^2} \gamma_R = 3\pi k_B T t_0 / \sigma^2$, corresponding to the friction parameters of a spherical particle in a Newtonian fluid with viscosity $\eta = 1 k_B T t_0 / \sigma$ (i.e., $\gamma_R = 8\pi\eta R^3$, $\gamma = 6\pi\eta R$). In Section **II B 3**, we choose the parameters to be the same as in a previous MIPS study without frictional contacts⁴³, i.e., $\gamma = \gamma_R / \sigma^2 = t_R k_B T / \sigma^2$ and $m = 0.05 k_B T (t_R / \sigma)^2$. Furthermore, the parameter ϵ in the WCA potential (Eq. (34)) is set to $\epsilon = k_B T$ in Sections **II B 1** and **II B 2**, and to $\epsilon = 10 k_B T$ in Section **II B 3**. The results presented in Sections **II B 1** and **II B 2** were acquired using HOOMD-blue⁴⁶, while those in Section **II B 3** were obtained with LAMMPS⁴⁷.

C. Data availability

The data that support the findings of this study are available from the corresponding author upon reasonable request.

D. Code availability

The simulation codes used to generate data (implemented in LAMMPS and HOOMD-blue) are available at <https://doi.org/10.48328/tudatalib-1838>.

-
- ¹ F. P. Bowden and D. Tabor, (No Title) (1973).
 - ² E. Popova and V. L. Popov, *Friction* **3**, 183 (2015).
 - ³ P. A. Cundall and O. D. Strack, *geotechnique* **29**, 47 (1979).
 - ⁴ T. Elperin and E. Golshtein, *Physica A* **242**, 332 (1997).
 - ⁵ H. J. Herrmann and S. Luding, *Continuum Mech. Thermodyn* **10**, 189 (1998).
 - ⁶ S. Luding, *Journal of Physics: Condensed Matter* **17**, S2623 (2005).
 - ⁷ P. G. d. Gennes, *Journal of Statistical Physics* **119**, 953 (2005).
 - ⁸ H. Touchette, E. Van der Straeten, and W. Just, *Journal of Physics A: Mathematical and Theoretical* **43**, 445002 (2010).
 - ⁹ A. Baule and P. Sollich, *Europhysics Letters* **97**, 20001 (2012).
 - ¹⁰ G. S. Agarwal, *Zeitschrift fur Physik* **252**, 25 (1972).
 - ¹¹ M. Semeraro, G. Gonnella, E. Lippiello, and A. Sarracino, *Symmetry* **15**, 200 (2023).
 - ¹² A. P. Antonov, L. Caprini, C. Scholz, and H. Löwen, arXiv preprint arXiv:2404.06615 (2024).
 - ¹³ N. J. Wagner and J. F. Brady, *Physics Today* **62**, 27 (2009), https://pubs.aip.org/physicstoday/article-pdf/62/10/27/16655247/27_1_online.pdf.
 - ¹⁴ R. Seto, R. Mari, J. F. Morris, and M. M. Denn, *Phys. Rev. Lett.* **111**, 218301 (2013).
 - ¹⁵ M. Wyart and M. E. Cates, *Physical review letters* **112**, 098302 (2014).
 - ¹⁶ B. van der Meer, T. Yanagishima, and R. Dullens, arXiv preprint arXiv:2209.12703 (2022).
 - ¹⁷ B. M. Guy, M. Hermes, and W. C. Poon, *Physical review letters* **115**, 088304 (2015).
 - ¹⁸ N. Y. Lin, B. M. Guy, M. Hermes, C. Ness, J. Sun, W. C. Poon, and I. Cohen, *Physical review letters* **115**, 228304 (2015).
 - ¹⁹ J. R. Royer, D. L. Blair, and S. D. Hudson, *Physical review letters* **116**, 188301 (2016).
 - ²⁰ J. Comtet, G. Chatté, A. Nigues, L. Bocquet, A. Siria, and A. Colin, *Nature communications* **8**, 15633 (2017).
 - ²¹ C.-P. Hsu, S. N. Ramakrishna, M. Zanini, N. D. Spencer, and L. Isa, *Proceedings of the National Academy of Sciences* **115**, 5117 (2018).
 - ²² J. F. Morris, *Annual Review of Fluid Mechanics* **52**, 121 (2020).
 - ²³ P. Nie, J. Chattoraj, A. Piscitelli, P. Doyle, R. Ni, and M. P. Ciamarra, *Physical Review E* **102**, 032612 (2020).
 - ²⁴ C. Abaurrea-Velasco, C. Lozano, C. Bechinger, and J. de Graaf, *Physical Review Letters* **125**, 258002 (2020).
 - ²⁵ N. Narinder, M. F. Bos, C. Abaurrea-Velasco, J. de Graaf, and C. Bechinger, *Soft Matter* **18**, 6246 (2022).
 - ²⁶ N. H. Nguyen, D. Klotsa, M. Engel, and S. C. Glotzer, *Physical review letters* **112**, 075701 (2014).
 - ²⁷ M. Fruchart, C. Scheibner, and V. Vitelli, *Annual Review of Condensed Matter Physics* **14**, 471 (2023).
 - ²⁸ H. Risken, *The Fokker-Planck Equation*, 2nd ed., Springer Series in Synergetics (Springer Berlin, Heidelberg, 1996).
 - ²⁹ W. Paul and J. Baschnagel, *Stochastic Processes*, 2nd ed. (Springer Berlin, Heidelberg, 2013).
 - ³⁰ P. Hänggi and H. Thomas, *Physics Reports* **88**, 207 (1982).
 - ³¹ Y. L. Klimontovich, *Physica A* **163**, 515 (1990).
 - ³² C. Escudero and H. Rojas, arxiv preprint arxiv:2309.03654 (2023), [10.48550/arXiv.2309.03654](https://doi.org/10.48550/arXiv.2309.03654).
 - ³³ P. Español and P. Warren, *Europhys. Lett.* **30**, 191 (1995).
 - ³⁴ C. Junghans, M. Praprotnik, and K. Kremer, *Soft Matter* **4**, 156 (2008).
 - ³⁵ J. D. Weeks, D. Chandler, and H. C. Andersen, *J. Chem. Phys.* **54**, 5237 (1971).
 - ³⁶ E. E. Keaveny, I. V. Pivkin, M. Maxey, and G. Em Karniadakis, *The Journal of Chemical Physics* **123**, 104107 (2005).
 - ³⁷ J. Smiatek, M. P. Allen, and F. Schmid, *Eur. Phys. J. E* **26**, 115 (2008).
 - ³⁸ J. Zhou, A. Belyaev, S. F., and O. Vinogradova, *J. Chem. Phys.* **136**, 194706 (2012).
 - ³⁹ J. A. Backer, C. P. Lowe, H. C. J. Hoefsloot, and P. D. Iedema, *J. Chem. Phys.* **122**, 154503 (2005).
 - ⁴⁰ D. A. Fedosov, G. E. Karniadakis, and B. Caswell, *J. Chem. Phys.* **132**, 144103 (2010).
 - ⁴¹ M. E. Cates and J. Tailleur, *Annual Review of Condensed Matter Physics* **6**, 219–244 (2015).
 - ⁴² H. Löwen, *The Journal of Chemical Physics* **152**, 040901 (2020).
 - ⁴³ L. Hecht, S. Mandal, H. Löwen, and B. Liebchen, *Physical Review Letters* **129**, 178001 (2022).
 - ⁴⁴ L. Hecht, K.-R. Dormann, K. L. Spanheimer, M. Ebrahimi, M. Cordts, S. Mandal, A. K. Mukhopadhyay, and B. Liebchen, *Computer Physics Communications* **309**, 109483 (2025).
 - ⁴⁵ I. M. Sokolov, *Chemical Physics* **375**, 359 (2010).

- ⁴⁶ J. A. Anderson, J. Glaser, and S. C. Glotzer, *Computational Materials Science* **173**, 109363 (2020).
- ⁴⁷ A. P. Thompson, H. M. Aktulga, R. Berger, D. S. Bolintineanu, W. M. Brown, P. S. Crozier, P. J. in 't Veld, A. Kohlmeyer, S. G. Moore, T. D. Nguyen, R. Shan, M. J. Stevens, J. Tranchida, C. Trott, and S. J. Plimpton, *Comp. Phys. Comm.* **271**, 108171 (2022).

V. ACKNOWLEDGMENTS

FS thanks Ralf Metzler for helpful discussions. This work was funded by the Deutsche Forschungsgemeinschaft (DFG) via Grant 233630050, TRR 146, Project A3, and A9. The authors gratefully acknowledge the computing time provided to them on the high-performance computer Mogon2 and Mogon NHR South-West.

VI. AUTHOR CONTRIBUTIONS

FS and BL designed the research and supervised the work. FS developed the theory with support from KH and KD. KH and KD implemented the simulation codes (HOOMD-blue and LAMMPS, respectively), performed the simulations, analyzed and visualized the data. All authors contributed to the writing of the original draft. KH and FS reviewed and finalized the manuscript.

VII. COMPETING INTERESTS

The authors declare no competing interests.

VIII. SUPPLEMENTARY INFORMATION

A. Deterministic two particle collision

In section II A 2, we analytically demonstrate that the deterministic friction force always reduces the kinetic energy of the particles during a collision. To validate this result, we simulated a collision between two particles in the absence of stochastic contact forces. Both particles have the radius $R = \sigma/2$ and mass $m = 1 k_B T(t_0/\sigma)^2$. The first particle is initially placed at the origin, while the second is positioned at $(1.15, 0.4, 0)\sigma$. The first particle has an initial velocity $v_x = \sqrt{3}\sigma/t_0$ in the x -direction and an initial angular velocity $\omega_z = 2 \cdot \sqrt{30}t_0^{-1}$ in z -direction, whereas the second particle is initially at rest. Both particles move freely and are not coupled to a thermostat. As shown in Fig. 9, the total energy E_{tot} decreases during the collision for all friction types, confirming our analytical prediction.

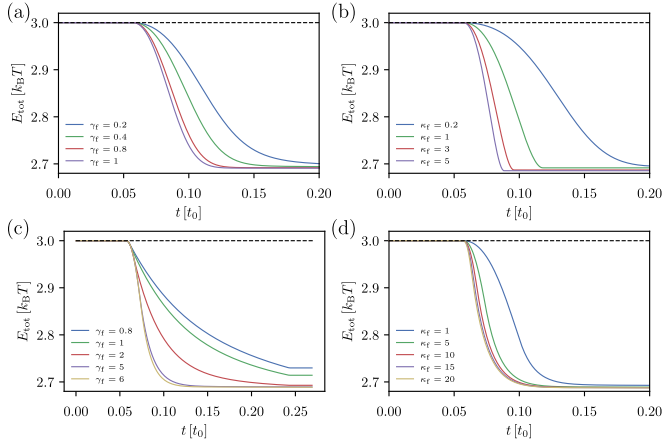


FIG. 9. E_{tot} total energy over time t for linear friction model (a) constant friction model (b) and Coulomb-Newton friction model with (c) fixed $\kappa_f = 5$ and varying γ_f , and (d) fixed $\gamma_f = 6 k_B T t_0 / \sigma^2$ and varying κ_f .

B. Thermodynamic consistency in models with frictional contact interactions

In section II B 1, we discuss the velocity and angular velocity histogram for a two-dimensional system with frictional contacts according to the constant friction model, which are used to determine the effective temperatures T_{eff} . Here we additionally show the corresponding histograms for both two-dimensional (Figure 10) and three-dimensional (Figure 11) systems with the linear friction model, the constant friction model, and the Coulomb-Newton friction model. The insets show the corresponding Kullback-Leibler divergence between the distribution obtained in simulations and the fitted Maxwell-Boltzmann distribution.

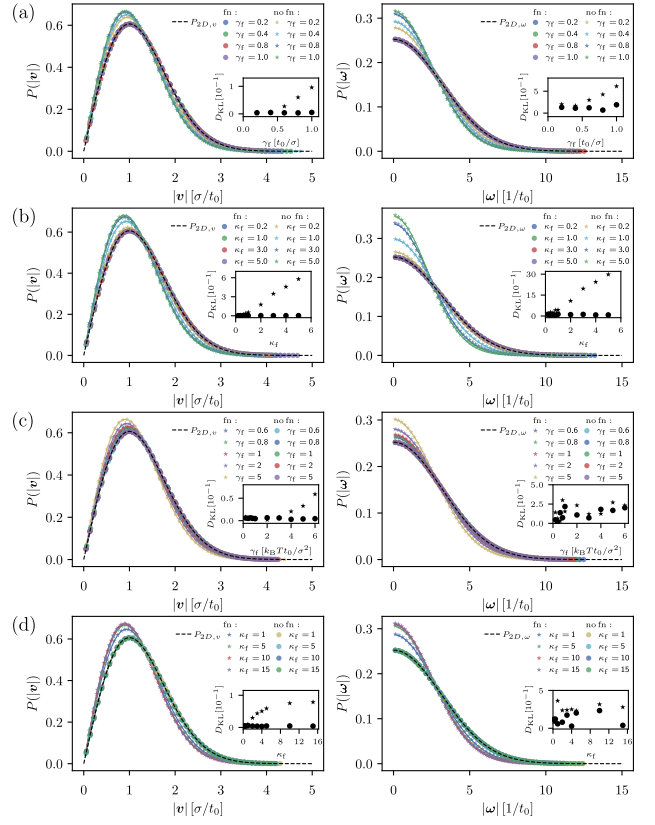


FIG. 10. (left) Velocity histograms and (right) angular velocity histograms for a two-dimensional passive colloid system with frictional contacts according to the (a) linear friction model (b) constant friction model (c,d) Coulomb-Newton friction model.

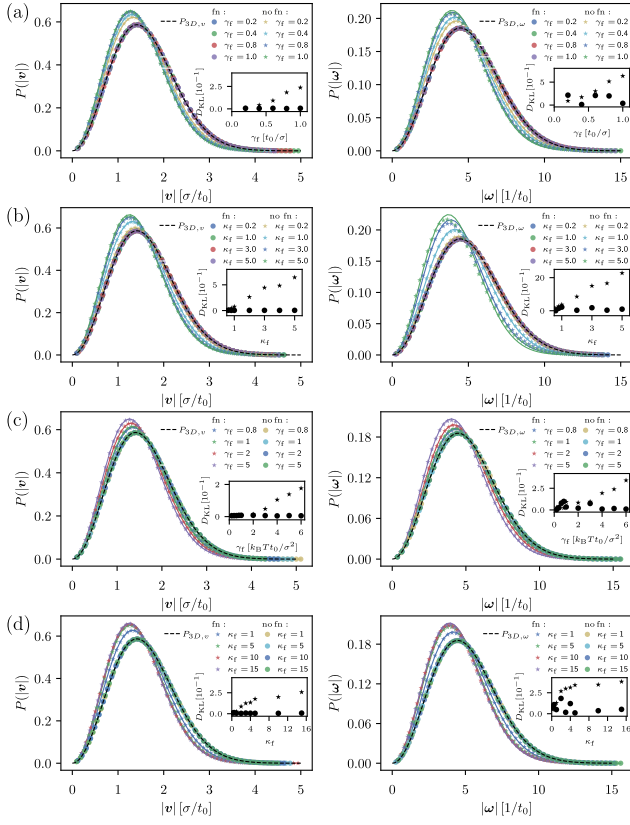


FIG. 11. (left) Velocity histograms and (right) angular velocity histograms for a three-dimensional passive colloid system with frictional contacts according to the (a) linear friction model (b) constant friction model (c,d) Coulomb-Newton friction model.

C. Pressure-driven flows

In section II B 2, we examine the dynamics of repulsive frictional particles under an external bulk force in a slit channel. Figure 12 displays the average particle velocity $v_{x,\text{eq}}$ along the direction of the bulk force for varying wall roughness parameters δ_w , measured after a simulation time t_{eq} . Our results show that the system reaches a stationary state by $t_{\text{eq}} = 500 t_0$ attaining a constant velocity, independent of further simulation time for each wall roughness parameters.

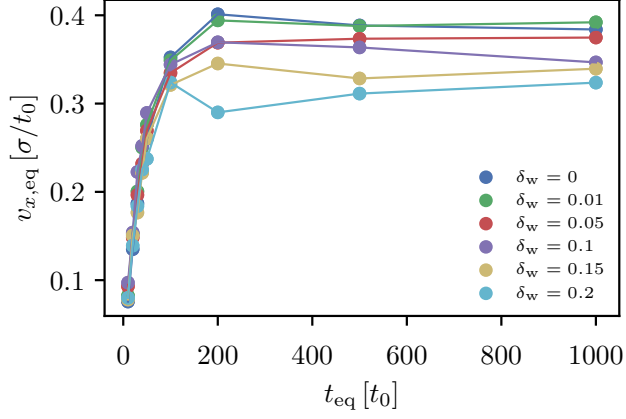


FIG. 12. Mean particle velocity $v_{x,\text{eq}}$ in the direction of the bulk force of particles for various wall roughness δ_w after the time t_{eq} .